Augmenting the spectral efficiency of enhanced PAM-DMT-based optical wireless communications

Augmenting the spectral efficiency of enhanced PAM-DMT-based optical wireless communications

Mohamed Sufyan Islim,* **and Harald Haas**

Institute for Digital Communications, Li-Fi R&D Centre, the University of Edinburgh, King's Buildings, Mayfield Road, Edinburgh, EH9 3JL, UK

*m.islim@ed.ac.uk

Abstract: The energy efficiency of pulse-amplitude-modulated discrete multitone modulation (PAM-DMT) decreases as the modulation order of *M*-PAM modulation increases. Enhanced PAM-DMT (ePAM-DMT) was proposed as a solution to the reduced energy efficiency of PAM-DMT. This was achieved by allowing multiple streams of PAM-DMT to be superimposed and successively demodulated at the receiver side. In order to maintain a distortion-free unipolar ePAM-DMT system, the multiple time-domain PAM-DMT streams are required to be aligned. However, aligning the antisymmetry in ePAM-DMT is complex and results in efficiency losses. In this paper, a novel simplified method to apply the superposition modulation on *M*-PAM modulated discrete multitone (DMT) is introduced. Contrary to ePAM-DMT, the signal generation of the proposed system, termed augmented spectral efficiency discrete multitone (ASE-DMT), occurs in the frequency domain. This results in an improved spectral and energy efficiency. The analytical bit error rate (BER) performance bound of the proposed system is derived and compared with Monte-Carlo simulations. The system performance is shown to offer significant electrical and optical energy savings compared with ePAM-DMT and DC-biased optical orthogonal frequency division multiplexing (DCO-OFDM).

OCIS codes: (060.4510) Optical communications; (170.4090) Modulation techniques; (220.4830) Systems design.

References and links

1. Cisco Visual Networking Index, "The Zettabyte era: trends and analysis," White Paper, Cisco (2015), `http://www.cisco.com/c/en/us/solutions/collateral/service-provider/visual-networking-index-vni/VNI_Hyperconnectivity_WP.pdf`.
2. S. Dimitrov and H. Haas, *Principles of LED Light Communications: Towards Networked Li-Fi*, (Cambridge University, 2015).
3. D. Tsonev, S. Videv, and H. Haas, "Towards a 100 Gb/s visible light wireless access network," Opt. Express **23**, 1627–1637 (2015).
4. J. Armstrong and A.J. Lowery, "Power efficient optical OFDM," Elect. Lett. **42**, 370–372 (2006).
5. S. C. J. Lee, S. Randel, F. Breyer, and A. M. J. Koonen, "PAM-DMT for intensity-modulated and direct-detection optical communication systems," IEEE Photonics Technology Letters **21**, 1749–1751 (2009).
6. D. Tsonev, S. Sinanovic, and H. Haas, "Novel unipolar orthogonal frequency division multiplexing (U-OFDM) for optical wireless," in *Proceedings of IEEE Vehicular Technology Conference (VTC Spring)*, (IEEE, 2012). pp. 1–5.
7. N. Fernando, Y. Hong; E. Viterbo, "Flip-OFDM for Unipolar Communication Systems," IEEE Tran. on Commun. **60**, 3726–3733 (2012).

8. D. Tsonev, S. Videv, and H. Haas, "Unlocking spectral efficiency in intensity modulation and direct detection systems," IEEE J. Sel. Areas Commun. **33**, 1758–1770 (2015).
9. M. Islim, D. Tsonev, and H. Haas, "Spectrally enhanced PAM-DMT for IM/DD optical wireless communications," in *Proceedings of IEEE Personal, Indoor, and Mobile Radio Communication*, (IEEE, 2015), pp. 877–882.
10. M. Islim, D. Tsonev, and H. Haas, "On the superposition modulation for OFDM-based optical wireless Communication," in *Proceedings of IEEE Global Signal and Information Processing conference*, (IEEE, 2015). pp. 1022–1026.
11. H. Elgala and T. Little, "SEE-OFDM: spectral and energy efficient OFDM for optical IM/DD systems," in *Proceedings of IEEE Personal, Indoor, and Mobile Radio Communication*, (IEEE, 2014), pp. 851–855.
12. Q. Wang, C. Qian, X. Guo, Z. Wang, D. G. Cunningham, and I. H. White, "Layered ACO-OFDM for intensity-modulated direct-detection optical wireless transmission," Opt. Express **23**, 12382–12393 (2015).
13. A.J. Lowery, "Enhanced asymmetrically-clipped optical OFDM," Opt. Express **24**, 3950–3966 (2016).
14. D. Tsonev, S. Sinanovic, and H. Haas, "Complete modelling of nonlinear distortion in OFDM-based optical wireless communication," J. Lightw. Technol. **31**, 3064–3076 (2013).
15. M. Islim, D. Tsonev, and H. Haas, "A generalized solution to the spectral efficiency loss in unipolar optical OFDM-based systems," in *Proceedings of IEEE International Conference on Communications (ICC)*, (IEEE, 2015). pp. 5126–3131.
16. F. Xiong, *Digital Modulation Techniques*, (Artech House Publishers, 2006), 2nd ed.
17. J. Proakis and G. Manolakis, *Digital Signal Processing* (Pearson, 2013), Chap. 8.
18. H. Hassanieh, P. Indyk, D. Katabi, and E. Price, "Nearly optimal sparse fourier transform," in *Proceedings of the forty-fourth annual ACM symposium on Theory of computing*, (ACM, 2012), pp. 563–578.
19. J. Armstrong and B. J. C. Schmidt, "Comparison of asymmetrically clipped optical OFDM and DC-biased optical OFDM in AWGN," IEEE Commun. Lett. **12**, 343–345 (2008).

1. Introduction

As the demand for higher data rate broadband access increases, the limited availability of the electromagnetic spectrum becomes an ever more important challenge. It is predicted that the annual global internet traffic will be in the order of the Zettabyte (1000 exabytes) by the end of 2016, and will be 2 Zettabytes per year by 2019 [1]. The increasing number of interconnected digital devices and online services highlights the necessity of new access technologies that could meet these demands. The visible light spectrum offers an abundant, unregulated communication bandwidth [2]. Visible light communication (VLC) is an emerging technique that is predicted to offer data rates of 100 Gb/s at very high deployment devices in the near future [3].

VLC is realized using off-the-shelf optoelectronic light emitting diodes (LEDs) and photodiodes (PDs). Due to the nature of these optoelectronic devices, the optical signal is required to be both real and positive. Optical orthogonal frequency division multiplexing (OFDM) is a promising candidate for high-speed VLCs and optical wireless communications (OWCs) [2]. Optical OFDM imposes Hermitian symmetry on the incoming frames to achieve a real time-domain waveform. The direct current (DC)-biased optical OFDM (DCO-OFDM) employs a DC bias to shift the signal samples to become positive. Unipolar OFDM schemes, such as asymmetrically clipped optical OFDM (ACO-OFDM) [4]; pulse-amplitude-modulated discrete multitone (PAM-DMT) [5]; unipolar orthogonal frequency division multiplexing (U-OFDM) [6]; and flip OFDM (FLIP-OFDM) [7], achieve unipolar OFDM time-domain waveforms by exploiting the frequency/time domain symmetries of the OFDM frames. As a result, all of these unipolar schemes, except PAM-DMT, have a reduced spectral efficiency in comparison with DCO-OFDM. The bit error rate (BER) performance of M-ary quadrature amplitude modulation (M-QAM) DCO-OFDM, should be compared with M^2-QAM {ACO-OFDM; U-OFDM; flipped-OFDM}, and M-PAM PAM-DMT. Since the BER performance of M-PAM is equivalent to the BER performance M^2-QAM at a given signal-to-noise ratio (SNR), the BER performance of all of the aforementioned unipolar OFDM schemes is identical. More importantly, the power efficiency of unipolar OFDM schemes decreases as the constellation size M increases, which makes it impracticable to employ these schemes for high data rate applications.

A novel superposition modulation technique termed, enhanced U-OFDM (eU-OFDM), was introduced in [8] as a solution to the spectral efficiency gap between U-OFDM and DCO-OFDM. Enhanced U-OFDM compensates for the spectral efficiency loss of U-OFDM by superimposing multiple U-OFDM frames. The superimposed U-OFDM streams are arranged so that the inter-stream-interference is null. The superposition concept was also extended to other unipolar OFDM techniques such as PAM-DMT in [9] and ACO-OFDM in [10–13]. The superposition optical OFDM techniques close the spectral efficiency gap between unipolar OFDM and DCO-OFDM, but require increased computational complexity and memory requirements. Enhanced asymmetrically clipped optical OFDM (eACO-OFDM) [10] utilizes the symmetry of ACO-OFDM subframes to allow multiple ACO-OFDM streams to be superimposed. A similar concept was also proposed by Elgala *et al.* [11] and Wang *et al.* [12] under the terms spectrally and energy efficient OFDM (SEE-OFDM), and layered asymmetrically clipped optical OFDM (Layered ACO-OFDM), respectively. The receiver proposed in SEE-OFDM [11] results in a SNR penalty that could have been avoided by using the symmetry properties of ACO-OFDM streams. The symmetry arrangement in Layered ACO-OFDM [12] is described in the frequency domain, however, it is shown in [12, Fig. 2] that it takes place in the time-domain. An alternative method to achieve superposition modulation based on aclaco was proposed by Lawery [13]. This is similar in principle to [10–12], however the superposition is performed in the frequency domain which results in simpler system implementation compared with the time domain processing of eACO-OFDM, SEE-OFDM and Layered ACO-OFDM. The constellation size of each superimposed depth in eACO-OFDM is optimized so that the full spectral efficiency of DCO-OFDM is achieved.

The enhanced pulse-amplitude-modulated discrete multitone (ePAM-DMT) [9] demonstrates that superposition modulation can also be utilized using the antisymmetry of PAM-DMT waveforms. However, aligning the antisymmetry of multiple PAM-DMT waveforms in the time domain is a complex process and results in spectral efficiency losses. The antisymmetry of PAM-DMT waveforms incorporates the cyclic prefix (CP) in aligning the symmetry. In addition ePAM-DMT requires flipping the PAM-DMT subframes in the time domain, which requires lengthy time-domain processing.

In this paper, a novel simplified technique is proposed to generate the superimposed PAM-DMT waveforms in the frequency domain, and it is termed augmented spectral efficiency discrete multitone (ASE-DMT). The proposed technique, ASE-DMT, avoids the spectral efficiency losses of ePAM-DMT and provides energy efficiency improvements over ePAM-DMT and DCO-OFDM by using the selective subcarrier modulation algorithm at each superimposed depth.

The paper is organized as follows. The proposed technique is described in Section 2, where the modulation concept of ASE-DMT and its spectral and power efficiencies are analysed. The theoretical analysis of the BER performance is derived in Section 3. A detailed study on the additional computation complexity of the proposed technique is presented in Section 4. A Performance comparison with ePAM-DMT and DCO-OFDM and simulation results of the proposed scheme are presented in Section 5. A simplified approach for implementing the proposed modulation technique is presented in Section 5.2. Finally, conclusions are given in Section 6.

2. Augmented spectral efficiency discrete multitone (ASE-DMT)

The augmented spectral efficiency discrete multitone (ASE-DMT) technique uses most of the available subcarriers in the OFDM frame. The ASE-DMT waveform can be generated by a selective loading of the imaginary and real components of the subcarriers. The waveform generation starts with a typical PAM-DMT [5] modulator at the first depth. Additional streams can only be superimposed on the first depth stream if their frequency domain subcarriers are

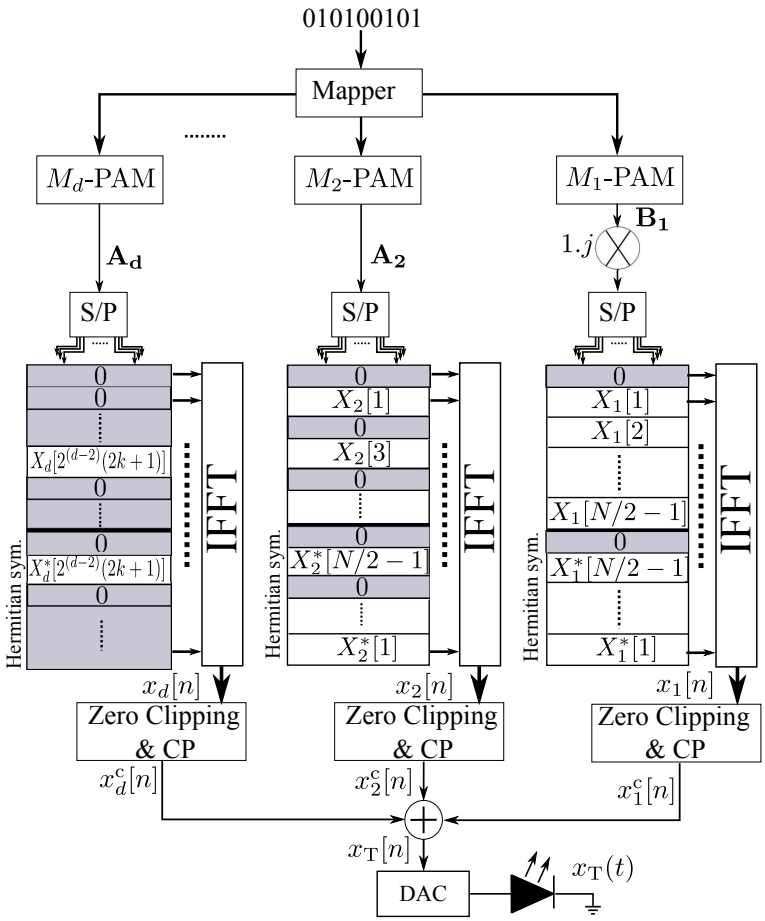

Fig. 1. ASE-DMT transmitter block diagram. $X_d[k]$ refers to the k^{th} subcarrier at depth d; S/P denotes for serial to parallel; DAC denotes for digital to analogue conversion; and CP refers to the cyclic prefixing.

loaded on the real components of the subcarriers. This constraint was fulfilled in ePAM-DMT by rearranging the ePAM-DMT time domain waveforms to have a Hermitian symmetry [9]. Alternatively, in ASE-DMT, the frames alignment is arranged in the frequency domain.

2.1. Modulation concept

The transmitter block diagram of ASE-DMT is shown in Fig. 1. At the first depth, the imaginary components of the subcarriers are loaded with M-ary pulse-amplitude modulation (M-PAM) symbols while the real components are kept unused $X_1[k] = jB_1[k]$, where $B_1[k]$ is the M-PAM symbol at the k^{th} subcarrier of depth 1. Note that Hermitian symmetry is also required in the frequency domain to guarantee a real time-domain output, $B_1[0] = B_1[N/2]$, and $B_1[k] = -B_1[N-k]$ for $k = 1, 2, ..., N/2-1$. As a result, the time domain PAM-DMT waveform $x_1[n]$

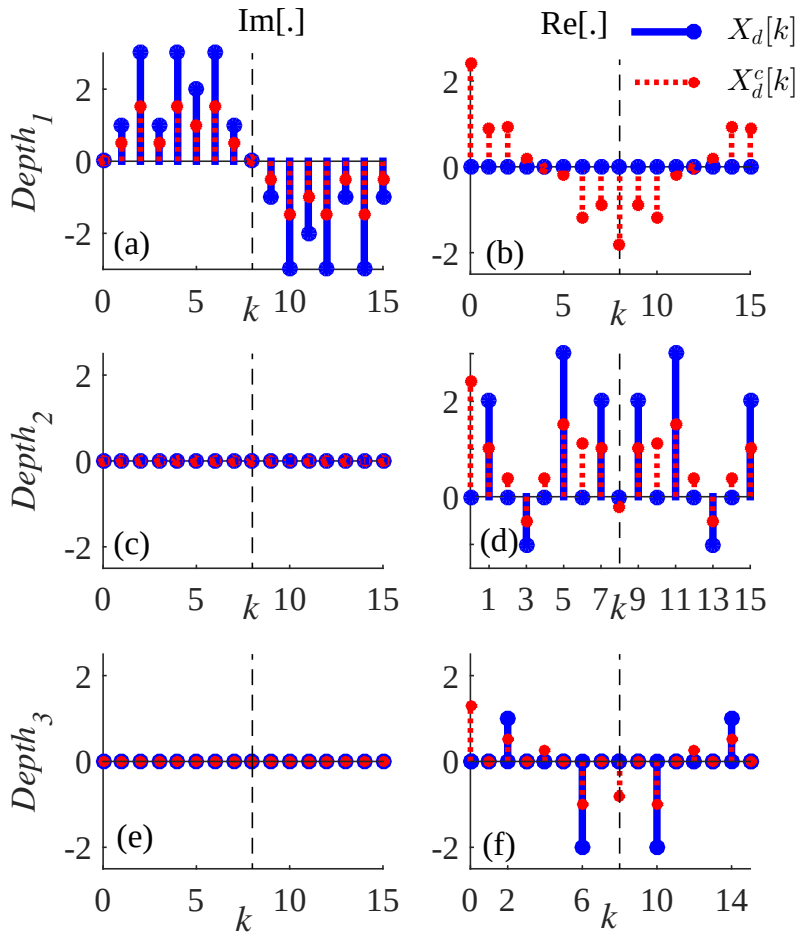

Fig. 2. An illustration of the frequency domain subcarrier loading at three depths ASE-DMT and the effects of zero clipping. (a) and (c) and (e) shows the imaginary components of the subcarriers before and after zero level time-domain clipping, $\Im[X_d[k]]$ and $\Im[X_d^c[k]]$, respectively. (b) and (d) and (f) shows the real components of the subcarriers before and after zero level time-domain clipping, $\Re[X_d[k]]$ and $\Re[X_d^c[k]]$, respectively.

can be written as:

$$x_1[n] = \frac{1}{\sqrt{N}} \sum_{k=0}^{N-1} X_1[k] e^{\frac{j2\pi kn}{N}}$$
$$= \frac{-2}{\sqrt{N}} \sum_{k=1}^{N/2-1} B[k] \sin \frac{2\pi kn}{N}. \quad (1)$$

It is straightforward to conclude that the time domain PAM-DMT waveform in (1) exhibits the following antisymmetry: $x_1[n] = -x_1[N-n]$, where $x_1[0] = x_1[N/2] = 0$. Following [14], the clipping at zero level is described as:

$$x_d^c[n] = \frac{x_d[n] + |x_d[n]|}{2}, \quad (2)$$

and the frequency domain transformation of the clipped waveform, $x_d^c[n]$, can be shown as:

$$X_d^c[k] = \frac{X_d[k] + \text{FFT}\{|x_d[n]|\}}{2}, \tag{3}$$

where the subscripts d denotes the depth d index, and $X_d[k] = \text{FFT}\{x_d[n]\}$. The effects of clipping on the subcarriers are shown in Fig. 2. Clipping of the negative samples at depth 1 is distortion-less to the information at the same depth because all of the distortion transforms into the real part of the subcarriers. As a simple proof, the distortion term $|x_1[n]|$ has a Hermitian symmetry $|x_1[n]| = |x_1[N-n]|$, which can also be proved by:

$$\begin{aligned}\text{FFT}\{|x_1[n]|\} &= \frac{1}{\sqrt{N}} \sum_{n=0}^{N-1} |x_1[n]| e^{-\frac{j2\pi kn}{N}} \\ &= \frac{2}{\sqrt{N}} \sum_{n=1}^{N/2-1} |x_1[n]| \cos\frac{2\pi kn}{N}.\end{aligned} \tag{4}$$

At depth 2, the odd subcarriers are loaded with real valued M-PAM symbols $X_2[k] = A_2[k]$, while all of the other subcarriers are kept unused. The subcarriers at depth 2, $X_2[k]$, can be written as:

$$X_2[k'] = \begin{cases} A_2[k'], & \text{if } k' = 2k+1 \\ 0, & \text{Otherwise} \end{cases}, \tag{5}$$

where $A_2[k']$ is the M-PAM symbol at the k'^{th} subcarrier of depth 2; and $k = 0, 1, ..., N/4-1$. Hermitian symmetry is also required to guarantee that $x_2[n]$ is real, $A_2[k] = A_2[N-k]$. As a result, the time domain waveform at depth 2, $x_2[n]$, would have the following symmetry: $x_2[n] = -x_2[n+N/2]$. Therefore, the distortion caused by clipping at zero level would only affect the real domain even subcarriers. This can be shown as:

$$\text{FFT}\{|x_2[n]|\} = \frac{1}{\sqrt{N}} \sum_{n=0}^{N/2-1} |x_2[k]| e^{-\frac{j2\pi kn}{N}} (1 + e^{-j\pi k}), \tag{6}$$

which takes values only at $X_2^c[2k]$, for $k = 0, 1, ..., N/2-1$. Therefore, the distortion is orthogonal to the information content at depth 1 and depth 2. Subsequent streams can be generated at depth d, where the subcarriers will be loaded with real valued M-PAM symbols:

$$X_d[k'] = \begin{cases} A_d[k'], & \text{if } k' = 2^{d-2}(2k+1) \\ 0, & \text{Otherwise} \end{cases}, \tag{7}$$

where $A_d[k']$ is the M-PAM symbol at the k'^{th} subcarrier of depth d; and $k = 0, 1, ..., N/2^d - 1$. Hermitian symmetry is also required to guarantee that $x_d[n]$ is real, $A_d[k] = A_d[N-k]$. Using (7), it can be shown that:

$$x_d[n] = -x_d[n + N/2^{d-1}] \quad \forall d > 1. \tag{8}$$

Using (3), $X_d[k]$ can be written as:

$$X_d[k] = \frac{1}{\sqrt{N}} \sum_{n=0}^{N/2^{d-1}-1} x_d[k] e^{-\frac{j2\pi kn}{N}} \kappa (1 - e^{\frac{-j\pi k}{2^{D-2}}}), \tag{9}$$

and the zero level clipping distortion effect on the subcarriers in the frequency domain can be written as:

$$\mathrm{FFT}\{|x_d[n]|\} = \frac{1}{\sqrt{N}} \sum_{n=0}^{N/2^{d-1}-1} |x_d[k]| e^{-\frac{j2\pi kn}{N}} \kappa (1 + e^{\frac{-j\pi k}{2^{D-2}}}), \tag{10}$$

where D is the total number of used depths, and κ can be written as:

$$\kappa = \prod_{d=2}^{D-1} (1 + e^{\frac{-j\pi k}{2^{d-2}}}). \tag{11}$$

Using (9) and (10), it can be shown that the zero level clipping is distortion-less to the information content at $X_d^{\mathrm{c}}[2^{d-2}(2k+1)]$, and that all of the distortion will affect the subcarriers at $X_d^{\mathrm{c}}[2^{d-1}k]$. Using this technique of selective subcarrier indexes loading at each depth will allow multiple M-PAM modulated waveforms to be superimposed without any inter-stream-interference. The active subcarriers of each superimposed depth will not be affected by the zero level clipping distortion of the current and subsequent depths. However, it will be affected by the distortion of the zero level clipping of the previous depths. This distortion will be estimated and cancelled at the receiver, as shown below.

After generating the time domain waveforms of all depths, the generated waveforms are clipped and the cyclic prefixes are prefixed. The overall ASE-DMT waveform can be obtained by superimposing the clipped waveforms of all depths:

$$x_{\mathrm{T}}[n] = \sum_{d=1}^{D} x_d^{\mathrm{c}}[n]. \tag{12}$$

Using (2) and (3), the ASE-DMT subcarriers can be written as:

$$X_{\mathrm{T}}[k] = \frac{jB_1[k] + \sum_{d=2}^{D} A_d[k] + \sum_{d=1}^{D} \mathrm{FFT}\{|X_d[n]|\}}{2}. \tag{13}$$

The information content of depth 1 can be obtained by considering only the imaginary components of the subcarriers. This can be given as $\hat{B}_1[k] = 2\Im(X_{\mathrm{T}}[k]) + W[k]$, where $W[k]$ is the frequency domain realization of the additive white Gaussian noise (AWGN) at the receiver [2]. The information of depth 1 can then be remodulated at the receiver to obtain $\hat{x}_1[n]$ which can be subtracted from the ASE-DMT received waveform, $x_{\mathrm{T}}[n]$. This would result in removing the imaginary component of $X_{\mathrm{T}}[n]$ and also removing the real domain distortion caused by the zero level clipping of the depth 1 waveform, $\mathrm{FFT}\{|x_1[n]|\}$. Subsequent depths can be demodulated by selecting the appropriate frequency subcarrier indexes at each depth. The real component of the subcarriers at $2^{d-2}(2k+1)$ for $k = 0, 1, ..., N/2^d - 1$ can then be remodulated to obtain the waveform at depth d, $\hat{x}_d[n]$, which would be subtracted from the remaining ASE-DMT waveform.

The same process is repeated until the information at the last depth is demodulated. In this way the distortion of the previous depths is estimated and cancelled from the higher depths in this successive receiver process.

2.2. Spectral efficiency

The spectral efficiency of the first depth of ASE-DMT is equivalent to the spectral efficiency of PAM-DMT, which is also similar to the spectral efficiency of DCO-OFDM. This can be written as:

$$\eta_{\mathrm{PAM}}(1) = \frac{\log_2(M_1)(N-2)}{2(N+N_{\mathrm{CP}})} \quad \text{bits/s/Hz}, \tag{14}$$

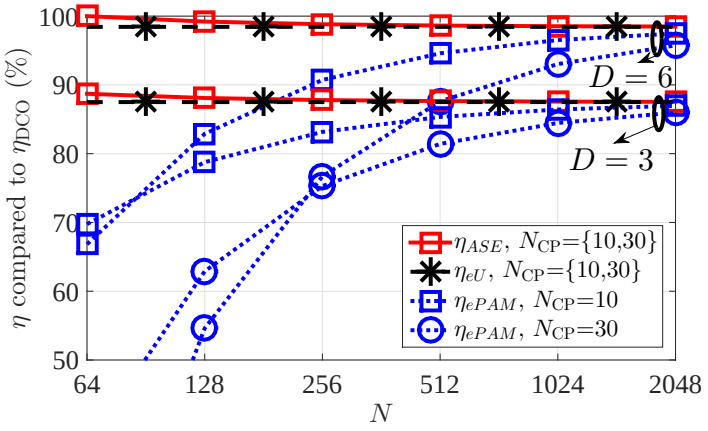

Fig. 3. The spectral efficiency of ASE-DMT, eU-OFDM, and ePAM-DMT compared to the spectral efficiency of DCO-OFDM for different FFT and CP lengths at $D = 3$ and $D = 6$.

where N is the FFT/inverse fast Fourier transform (IFFT) frame length, M_1 is the constellation size at first depth of ASE-DMT, and N_{CP} is the cyclic prefix length. The spectral efficiency of higher depths $d \geq 2$ can be expressed as:

$$\eta_{\text{PAM}}(d) = \frac{\log_2(M_d)N}{2^d(N+N_{\text{CP}})} \quad \text{bits/s/Hz}, \tag{15}$$

where M_d is the constellation size at depth d. As a result, the spectral efficiency of ASE-DMT can be calculated as:

$$\begin{aligned}\eta_{\text{ASE}}(D) &= \sum_{d=1}^{D} \eta_{\text{PAM}}(d) \quad \text{bits/s/Hz} \\ &= \frac{\log_2(M_1)(N-2) + \sum_{d=2}^{D} \frac{\log_2(M_d)(N)}{2^{d-1}}}{2(N+N_{\text{CP}})}.\end{aligned} \tag{16}$$

The spectral efficiency ratio of ASE-DMT to the spectral efficiency contribution of each individual depth can be written as:

$$\alpha_\eta(D,d) = \frac{\eta_{\text{ASE}}(D)}{\eta_{\text{PAM}}(d)2^{d-1}}. \tag{17}$$

The spectral efficiency of ASE-DMT approaches twice the spectral efficiency of DCO-OFDM as the total number of depths increase. However, the energy efficiency comparison of both modulation schemes should be considered at an equivalent spectral efficiency. Therefore, the superimposed waveforms in ASE-DMT use smaller constellation sizes, $M_d = \sqrt{M_{\text{DCO}}}$, that can build-up a DCO-OFDM equivalent spectral efficiency. Since the system design of ePAM-DMT employs the cyclic prefixes in the symmetry alignment of the PAM-DMT time-domain frames, the spectral efficiency of ePAM-DMT is a function of the FFT/IFFT frame and cyclic prefix sizes.

The spectral efficiency of ePAM-DMT tends to increase as the FFT/IFFT frame size increases. Unlike ePAM-DMT, the spectral efficiency of ASE-DMT is independent of the cyclic prefix length and therefore, can be employed with smaller FFT/IFFT sizes. The spectral efficiency ratio of ASE-DMT, ePAM-DMT and eU-OFDM to the spectral efficiency of DCO-OFDM is shown in Fig. 3. The spectral efficiency of ASE-DMT is slightly higher than the

spectral efficiency of eU-OFDM at small FFT/IFFT sizes. It is shown that when $D = 6$ and $N = 64$, the spectral efficiency of ASE-DMT exactly matches the spectral efficiency of DCO-OFDM.

2.3. Power efficiency

The real bipolar OFDM time-domain waveform can be approximated with a Normal distribution, $x(t) \sim \mathcal{N}(0, \sigma_{\mathrm{x}}^2)$ when $N \geq 64$, where σ_{x} is the standard deviation of $x(t)$ [2]. It was shown in [14] that PAM-DMT follows a truncated normal distribution. The stream at depth D is scaled by a parameter $1/\gamma_d$ to facilitate the optimization of the allocated power at that stream. The ASE-DMT time-domain waveform at depth d follows a truncated normal distribution with a mean $\mathrm{E}[\mathrm{x}_d(t)] = \phi(0)\sigma_{\mathrm{x}}/(\gamma_d\sqrt{2^{d-1}})$, where $1/\gamma_d$ is the scaling factor at depth d, $\mathrm{E}[\cdot]$ is a statistical expectation, and $\phi(x)$ is the probability density function (PDF) of the standard normal distribution. As a result, the average electrical and optical power of ASE-DMT is equivalent to the electrical and optical power of eU-OFDM which can be written as [15]:

$$\begin{aligned} P_{\mathrm{Ele}}^{\mathrm{avg}}(D, \underline{\gamma}) &= \mathrm{E}\left[x_{\mathrm{T}}^2(t)\right] = \mathrm{E}\left[\left(\sum_{d=1}^{D} x_d(t)\right)^2\right] \\ &= \sigma_{\mathrm{s}}^2\left(\sum_{d=1}^{D}\frac{\gamma_d^{-2}}{2^d} + 2\phi^2(0)\sum_{d_1=1}^{D}\sum_{\substack{d_2=1 \\ d_1\neq d_2}}^{D}\frac{(\gamma_{d_1}\gamma_{d_2})^{-1}}{\sqrt{2^{d_1+d_2}}}\right), \end{aligned} \tag{18}$$

$$P_{\mathrm{Opt}}^{\mathrm{avg}}(D, \underline{\gamma}) = \sum_{d=1}^{D}\mathrm{E}[\mathrm{s}_d(t)] = \phi(0)\sigma_{\mathrm{s}}\sum_{d=1}^{D}\frac{\gamma_d^{-1}}{\sqrt{2^{d-1}}}, \tag{19}$$

where $x_{\mathrm{T}}(t)$ is the time domain ASE-DMT waveform; $x_d(t)$ is the time domain PAM-DMT at depth d; and $\underline{\gamma} = \{\gamma_d^{-1}; d = 1, 2, \ldots, D\}$ is the set of scaling factors applied to each corresponding stream. The ratio of the average electrical power of ASE-DMT waveform to the average electrical power of a PAM-DMT stream, $P_{\mathrm{Ele},d}^{\mathrm{avg}}(\gamma_d) = \sigma_{\mathrm{x}}^2/(2\gamma_d^2)$, is given by:

$$\alpha_{\mathrm{Ele}}^{P}(D, \underline{\gamma}) = \frac{P_{\mathrm{Ele}}^{\mathrm{avg}}(D, \underline{\gamma})}{P_{\mathrm{Ele},d}^{\mathrm{avg}}(\gamma_d)}. \tag{20}$$

3. Theoretical BER analysis

The ASE-DMT received signal is given by:

$$\mathbf{y} = \mathbf{H}\mathbf{x} + \mathbf{w}, \tag{21}$$

where $\mathbf{x}$ and $\mathbf{y}$ are the transmitted and received ASE-DMT waveforms; $\mathbf{w} = \{w_i; i = 0, 1, ..., N-1\}$ is the AWGN samples, $w_i \sim \mathcal{N}(0, N_o)$, where N_o is the double-sided power spectral density (PSD) of the noise at the receiver; and $\mathbf{H}$ is a $N \times N$ circulant convolution channel matrix with the first column representing the channel impulse response $\mathbf{h} = [h_0, h_1, ..., h_L, 0, ..., 0]^{\mathrm{T}}$, where L is the number of channel taps. The channel matrix $\mathbf{H}$ can be diagonalized as:

$$\mathbf{H} = \mathbf{F}^{*}\mathbf{\Lambda}\mathbf{F}, \tag{22}$$

where $\mathbf{F}$ is an $N \times N$ Discrete Fourier transform (DFT) matrix, and $\mathbf{\Lambda}$ is an $N \times N$ diagonal matrix with the eigenvalues of the channel $\mathbf{\Lambda} = [\Lambda_0, \Lambda_1, ..., \Lambda_N]^{\mathrm{T}}$.

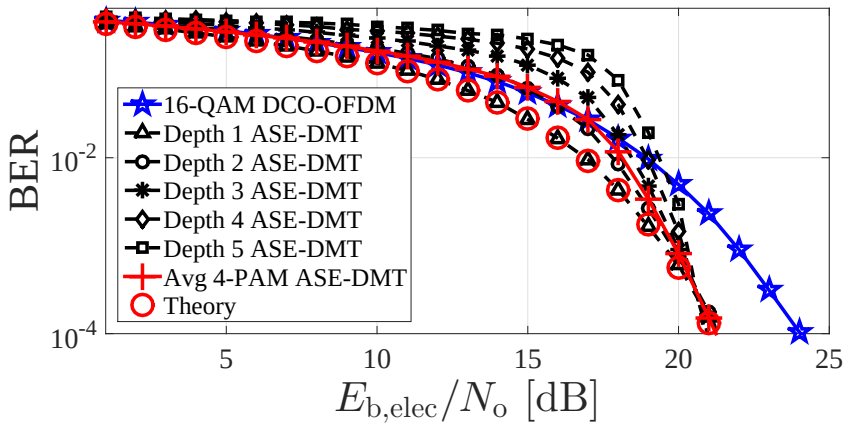

Fig. 4. The BER performance of 16-QAM ASE-DMT depths with a total number of depths $D = 5$. The BER of DCO-OFDM is only shown for comparison purposes.

The theoretical BER performance of ASE-DMT can be derived using the analytical BER performance of real M-QAM OFDM [16]. However, the SNR should be scaled by half to compensate for the energy loss of zero level clipping at each depth. This is consistent with the 3 dB loss of the BER performance of PAM-DMT. In addition, the SNR should also be scaled by the energy loss per bit incurred by the superposition modulation of ASE-DMT, which can be written as:

$$\alpha_{\mathrm{Ele}}(D,d,\underline{\gamma}) = \frac{\alpha^{P}_{\mathrm{Ele}}(D,\underline{\gamma})}{\alpha_{\eta}(D,d)}. \tag{23}$$

Since the BER performance of M-PAM is equivalent to the BER performance of M^2-QAM in an AWGN channel, the analytical BER performance bound of ASE-DMT in the AWGN channel can be derived as:

$$\mathrm{BER}_{(D,d,\underline{\gamma})} \cong \frac{2}{\log_2(M_d)}\left(1-\frac{1}{M_d}\right) \times \sum_{l=1}^{2}\sum_{k=1}^{N} \mathrm{Q}\left((2l-1)\sqrt{\frac{3|\Lambda_k|^2 E_{\mathrm{b,elec}}\log_2(M_d)}{N_{\mathrm{o}}\alpha_{\mathrm{Ele}}(D,d,\underline{\gamma})(M_d^2-1)}}\right), \tag{24}$$

where $E_{\mathrm{b,elec}}/N_{\mathrm{o}}$ is the electrical SNR of real M-QAM OFDM, and N_{o} is the double side noise PSD. An equivalent bound for the ASE-DMT BER performance as a function of the optical SNR can be established by scaling the electrical SNR, $E_{\mathrm{b,elec}}/N_{\mathrm{o}}$ in (24), with the ratio of electrical average power (18) to the optical average power (19).

As shown in Fig. 4, the analytical performance bound matches the BER performance of the first depth. The BER performance of other depths tends to be affected by the wrongly decoded bits at the lower order depths. Any incorrectly decoded bit at the lower order depths translates into further incorrect bits at higher order depths. However, at high SNR, the BER performance of all depths converges to match with the analytical performance of ASE-DMT.

As shown in Fig. 4, the BER performance of 4-PAM ASE-DMT is more efficient, with a 3 dB gain, than 16-QAM DCO-OFDM in terms of the electrical energy efficiency. The spectral efficiency ratio of ASE-DMT to the spectral efficiency of DCO-OFDM is 97%.

4. Computational complexity

The computation complexity of ASE-DMT and ePAM-DMT are studied and compared with the computation complexity of DCO-OFDM in this section. The computation complexity is

dominated by the number of multiplications in FFT/IFFT operations. Therefore, the computation complexity in this paper is defined as the number of complex multiplications required to perform a FFT/IFFT operation.

4.1. Computation complexity of DCO-OFDM

At the transmitter side, DCO-OFDM requires N-point complex multiplications which result in a computation complexity of $\mathscr{O}(N\log_2(N))$. The FFT operation at the receiver side of DCO-OFDM is performed on real-valued frames. Two N-point FFT operations on two real-valued signals can be realized using one N-point FFT on one complex-valued signal [17]. Therefore, the computation complexity at the receiver of DCO-OFDM is $\mathscr{O}(N/2\log_2(N))$. The computation complexity per bit of DCO-OFDM can be written as:

$$C_{\text{DCO}} = \frac{2\mathscr{O}(3N/2\log_2(N))}{\log_2(M_{\text{DCO}})(N-2)}, \tag{25}$$

where M_{DCO} is the constellation size of DCO-OFDM.

4.2. Computation complexity of ASE-DMT

At the transmitter side of PAM-DMT, an IFFT operation is applied on imaginary-valued frames. At the receiver side, a single FFT operation is applied on real-valued frames. Therefore, the computation complexity of PAM-DMT for each of the transmitter and receiver is $\mathscr{O}(N/2\log_2(N))$.

The first depth of ASE-DMT has a computation complexity similar to the computation complexity of a PAM-DMT transmitter. Higher depths of ASE-DMT are sparse as they have a low number of active subcarriers. The number of active subcarriers at depth d is: $N/2^{d-1}$, $\forall d \leq 2$. Therefore, the IFFT operation at higher order depths $d \leq 2$, can be optimized to avoid the calculations performed on zeros. Given that the subcarriers in these depths are real-valued, the computation complexity at the transmitter of depth d is $\mathscr{O}(N/2^d\log_2(N))$. Therefore, the computation complexity of ASE-DMT transmitter is given as:

$$\begin{aligned} C_{\text{ASE}}^{\text{Tx}} &= \mathscr{O}(N/2\log_2(N)) + \sum_{d=2}^{D}\mathscr{O}(N/2^d\log_2(N)) \\ &\approx \mathscr{O}(N\log_2(N)), \end{aligned} \tag{26}$$

where D is the total number of depths.

The first demodulation process at the receiver of ASE-DMT is applied on real-valued frames, therefore, the computation complexity associated with this process is equivalent to the computation complexity of a DCO-OFDM receiver. All the other demodulation process are also applied on real-valued frames. However, the frames at higher order depths are sparse in the frequency domain. A specific set of subcarriers is only required at the output of each demodulation process. Therefore, the FFT operation at higher order depths, $d \leq 2$, is only evaluated at subcarriers given by (7). Algorithms such as Sparse FFT [18] can also be applied for depth d with a computational complexity of $\mathscr{O}(N/2^d\log_2(N))$. The demodulated streams for all depths, except the last one, are required to be remodulated at the receiver. The associated complexity of remodulating the first depth is: $\mathscr{O}(N/2\log_2(N))$, and the associated complexity of remodulating other depths is $\sum_{d=2}^{D}\mathscr{O}(N/2^d\log_2(N))$. Therefore, the computation complexity of a ASE-DMT receiver is given as:

$$\begin{aligned} C_{\text{ASE}}^{\text{Rx}} &= \mathscr{O}(N/2\log_2(N)) + \sum_{d=2}^{D}\mathscr{O}(N/2^d\log_2(N)) + \sum_{d=2}^{D-1}\mathscr{O}(N/2^d\log_2(N)) \\ &\approx \mathscr{O}(2N\log_2(N)). \end{aligned} \tag{27}$$

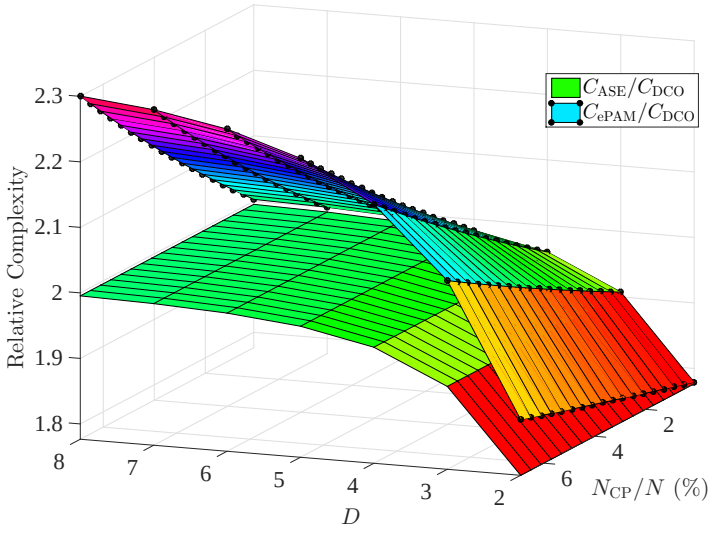

Fig. 5. The relative computation complexity of ASE-DMT and ePAM-DMT in comparison with the computation complexity of DCO-OFDM as a function of the total number of depths D, and the cyclic prefix percentage of the frame size N_{CP}/N.

The computation complexity of ASE-DMT per bit is given as:

$$C_{\mathrm{ASE}} = \frac{2(C_{\mathrm{ASE}}^{\mathrm{Tx}} + C_{\mathrm{ASE}}^{\mathrm{Rx}})}{\log_2(M_d)(N-2) + \sum_{d=2}^{D} \log_2(M_d) N/2^{d-1}}, \tag{28}$$

where M_d is the constellation size used for all depths in ASE-DMT, $M_d = \sqrt{M_{\mathrm{DCO}}}$.

4.3. Computation complexity of ePAM-DMT

The cyclic prefix at each depth of ePAM-DMT is used in the symmetry alignment of superimposed depths. This reduces the frame sizes at higher order depths. The FFT frame size at depth-d of ePAM-DMT is given as $N_d = N_{d-1} - 2N_{\mathrm{CP}} - 2$, $\forall d \geq 2$, where $N_1 = N$, and N is the frame size of DCO-OFDM. The frame sizes of all depths in ePAM-DMT are zero-padded to the next power of two.

At the transmitter side of ePAM-DMT, $\sum_{d=1}^{D} 2^{d-1}$ PAM-DMT frames are required to generate 2^{D-1} ePAM-DMT frames. Therefore, the computation complexity of the ePAM-DMT transmitter can be given as:

$$\begin{aligned} C_{\mathrm{ePAM}}^{\mathrm{Tx}} &= \sum_{d=1}^{D} 2^{d-D} \mathscr{O}(N/2 \log_2(N)) \\ &\approx \mathscr{O}(N \log_2(N)). \end{aligned} \tag{29}$$

This is equivalent to the computation complexity of DCO-OFDM transmitter.

At the receiver side of ePAM-DMT, $\sum_{d=1}^{D} 2^{d-1}$ PAM-DMT frames are required to be demodulated and $\sum_{d=2}^{D} 2^{d-1}$ PAM-DMT frames are required to be remodulated in order for 2^{D-1} frames of ePAM-DMT to be demodulated. Therefore, the computation complexity of

the ePAM-DMT receiver can be given as:

$$C_{\text{ePAM}}^{\text{Rx}} = \frac{\mathcal{O}(N/2\log_2(N)) + 2\sum_{d=2}^{D} 2^{d-1}\mathcal{O}(N/2\log_2(N))}{2^{D-1}}$$
$$\approx \mathcal{O}(2N\log_2(N)), \tag{30}$$

which is equivalent to twice the computation complexity of DCO-OFDM transmitter. Therefore the computation complexity of ePAM-DMT per bit is given as:

$$C_{\text{ePAM}} = \frac{2(C_{\text{ePAM}}^{\text{Tx}} + C_{\text{ePAM}}^{\text{Rx}})}{\log_2(M)(N-2) + \sum_{d=2}^{D}\log_2(M)N_d/2^{d-1}}, \tag{31}$$

where N_d is the frame size at depth-d and M is the constellation size used for all depths in ePAM-DMT, $M = \sqrt{M_{\text{DCO}}}$.

4.4. Computation complexity comparison

The ratio of the computation complexities per bit of ASE-DMT to DCO-OFDM, $C_{\text{ASE}}/C_{\text{DCO}}$, and the the ratio of the computation complexities per bit of ePAM-DMT to DCO-OFDM, $C_{\text{ePAM}}/C_{\text{DCO}}$. are presented in Fig. 5 as a function of the total number of used depths D and the cyclic prefix percentage of the overall frame size N_{CP}/N. The relative complexity of ASE-DMT is independent of the cyclic prefix and it increases as the total number of depths increases. However, it converges to twice the complexity of DCO-OFDM.

Table 1. Computational complexity of the Transmitter and receiver of DCO-OFDM, ePAM-DMT and ASE-DMT.

Modulation technique	Computational complexity	
	Transmitter	Receiver
DCO-OFDM	$\mathcal{O}(N\log_2(N))$	$\mathcal{O}(N/2\log_2(N))$
ASE-DMT	$\mathcal{O}(N\log_2(N))$	$\mathcal{O}(2N\log_2(N))$
ePAM-DMT	$\mathcal{O}(N\log_2(N))$	$\mathcal{O}(2N\log_2(N))$

The relative complexity of ePAM-DMT increases as the cyclic prefix length increases and as the total number of depths increases. The relative complexity of ePAM-DMT has a lower bound that is equivalent to the relative complexity of ASE-DMT when the cyclic prefix length is zero. The cyclic prefix length is limited by the total number of depths used. The maximum cyclic prefix length for $D = 8$ is only 8% of the OFDM frame size. When the cyclic prefix is 8%, the relative complexity of ePAM-DMT is 2.3 times the complexity of DCO-OFDM. The computation complexities of DCO-OFDM, ePAM-DMT and ASE-DMT are summarized in Table 1.

4.5. Practical considerations

The transmission cannot be started in ePAM-DMT, unless $2^D - 1$ PAM-DMT frames are available at the transmitter side. In addition, frames at higher order depths are required to be processed in the time domain to achieve the symmetry required for superposition modulation. This introduces additional delay at the transmitter side. At the receiver side of ePAM-DMT, the demodulation of frames at depth-d can only happen after all lower depths have been demodulated and remodulated. This is estimated at $\sum_{d'=2}^{d} 2^{D-d'+1}$ PAM-DMT frames. Moreover, 2^D frames are required to be buffered at the receiver, until the demodulation process of a full ePAM-DMT frame finishes.

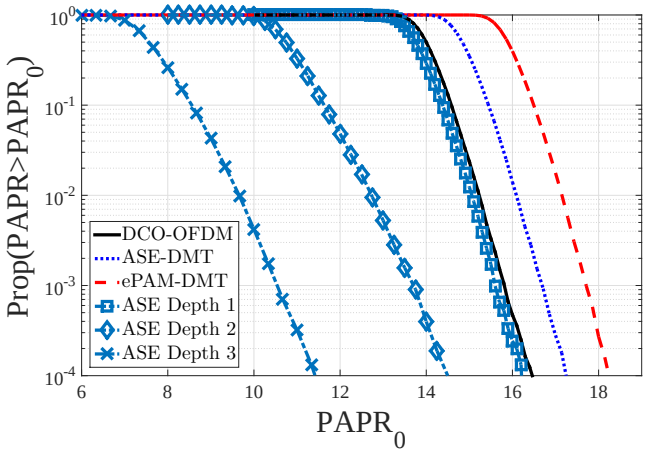

Fig. 6. The peak to average power ratio of ASE-DMT (depths and overall), ePAM-DMT and DCO-OFDM.

There is no delay associated with the ASE-DMT transmitter, as all of the depths are generated at the same time. At the receiver side of ASE-DMT, the demodulation of frames at depth-d can only take place after all of the lower depths have been demodulated and remodulated. This is estimated at $(d-1)$ PAM-DMT frames. Moreover, $(d-1)$ frames are required to be buffered at the receiver, until the demodulation process of a full ASE-DMT frame finishes.

The spectral efficiency of each additional stream decreases exponentially. Therefore, it is more efficient to implement ASE-DMT with small number of depths, $D=2$ or $D=3$. This would result in a small spectral efficiency gap between ASE-DMT and DCO-OFDM, 12.5% of the spectral efficiency of DCO-OFDM when $D=3$. A solution to this issue is given in Section 5.2

5. Performance comparison

Typical OFDM signals attain high peak-to-average power ratios (PAPRs). This drives the LEDs into non-linear regions because of their limited dynamic range. However, the higher order depths in ASE-DMT are sparse in the frequency domain. This reduces the PAPR of higher order depths. To exploit this property, the waveform at each depth can be used to drive a single LED in an LED array. This allows the waveforms to be superimposed in the optical domain and reduces the PAPR, and this will mitigate any non-linearity. The PAPR of ASE-DMT depths is presented in Fig. 6 to illustrate the sparsity effect on the PAPR. The PAPR of ASE-DMT depths increases as the depth order, d, increases. The PAPR of the overall ASE-DMT waveform is shown to be higher than the PAPR of DCO-OFDM but lower than the PAPR of ePAM-DMT.

The BER performance of ASE-DMT is compared with the BER performance of ePAM-DMT and DCO-OFDM in an AWGN channel. An ideal LED model is used, therefore, the only non-linear operation considered is the clipping at the zero level. The DC bias is defined to be a multiple of the standard deviation of the bipolar OFDM signal $k_{M_{\mathrm{DCO}}}\sigma_s$. The energy dissipation of DCO-OFDM compared with bipolar OFDM can be written as [19]:

$$B_{\mathrm{DC}}^{\mathrm{dB}} = 10\log_{10}(k_{M_{\mathrm{DCO}}}^2+1). \tag{32}$$

The DC bias for DCO-OFDM is estimated through Monte-Carlo simulations. Since the BER performance of $\sqrt{M}$-PAM is equivalent to the BER performance of M-QAM at a given SNR, it would not be possible for ASE-DMT to achieve the spectral efficiency of a non-squared

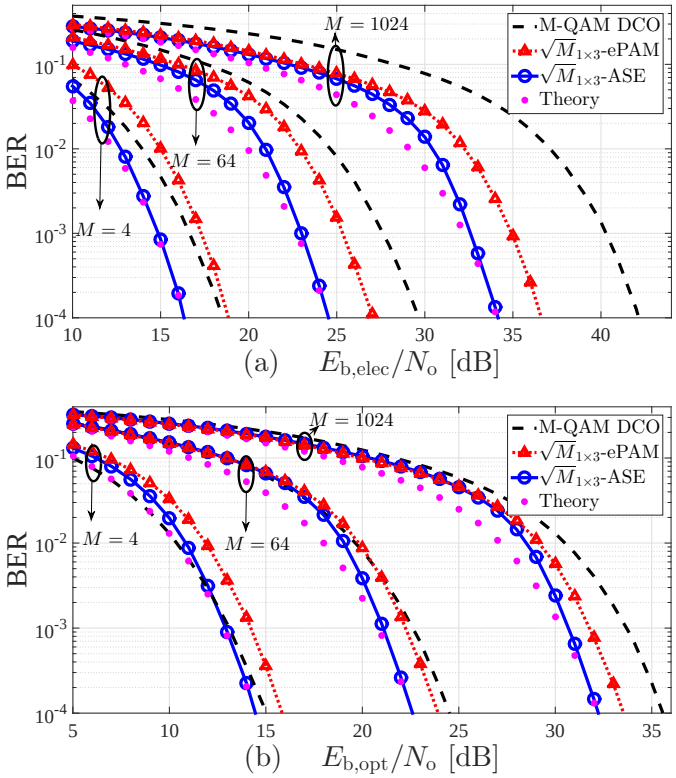

Fig. 7. The BER performance comparison of ASE-DMT, ePAM-DMT, and DCO-OFDM for different spectral efficiencies in an AWGN channel as a function of: (a) electrical SNR, and (b) optical SNR. The DC biasing levels for DCO-OFDM at $M = \{4, 64, 1024\}$ are estimated through Monte Carlo simulations at respectively 6 dB, 9.5 dB, and 13 dB as described in (32).

M-QAM constellation size. When equal constellation size is used at each modulation depth of ASE-DMT, only integer spectral efficiencies, $\eta_{\text{ASE}}(D) = \{1, 2, 3, ...\}$ bits/s/Hz, can be achieved.

5.1. Simulation results

The BER performance of the proposed scheme $\sqrt{M}$-PAM ASE-DMT is compared with the BER performance of $\sqrt{M}$-PAM ePAM-DMT and M-QAM DCO-OFDM as functions of the electrical SNR in an AWGN channel at Fig. 7(a). The proposed scheme, ASE-DMT, is more energy efficient than ePAM-DMT and DCO-OFDM for all of the presented cases as a function of the electrical SNR. At different spectral efficiencies, the electrical energy savings ASE-DMT are between 2.24 dB and 8 dB when compared with DCO-OFDM, and almost constant at 2.5 dB when compared with ePAM-DMT at a BER of 10^{-4}. Similar trends are shown in Fig. 7 (b) for the optical SNR. At different spectral efficiencies, the optical energy savings of ASE-DMT are between 0.6 dB and 3.25 dB when compared with DCO-OFDM, and are almost constant at 1.3 dB when compared with ePAM-DMT at a BER of 10^{-4}. The energy efficiency gains of ASE-DMT over DCO-OFDM at different spectral efficiencies are summarized in Table 2.

ASE-DMT is more efficient than ePAM-DMT in terms of both the electrical and optical SNR. This is due to the fact that in ePAM-DMT half of the frames are removed after each

demodulation process [9]. The frequency domain loading of M-PAM symbols in ASE-DMT does not require this process, which results in a performance gain of ASE-DMT over ePAM-DMT.

The theoretical BER bounds underestimate the BER at lower SNR due to the propagation errors in the successive streams cancellation process at the receiver. However, the theoretical BER bounds match the Monte-Carlo simulation results at high SNR values.

Table 2. Energy efficiency gains of ASE-DMT over DCO-OFDM at a BER of 10^{-4}.

Spectral efficiency [bits/s/Hz]	Electrical energy gains [dB]	Optical energy gains [dB]
1	2.24	0.6
2	4	1.7
3	5	2
4	5.75	2.5
5	8	3.25

Note that the BER performance of ASE-DMT is identical to the BER performance of eU-OFDM [8], and to the BER performance of eACO-OFDM [10] when identical constellation size and unitary scaling factors are used for eACO-OFDM. This is an unsurprising result, because the BER performance of their unipolar OFDM based-schemes forms (PAM-DMT, U-OFDM, and ACO-OFDM) is also identical [14]. A detailed comparison between the superposition OFDM modulation schemes will be the subject of future research on this topic.

The performance difference between ASE-DMT and DCO-OFDM is almost equivalent for both flat channels and frequency selective channels. When subjected to the same communication channel, the individual subcarriers between the OFDM-based techniques are subjected to the same attenuation by the channel. As a result, the SNR penalty due to the channel in both techniques is the same. The results for a frequency selective channel are only valid for the specific channel conditions, which are specific to the communication scenario. Therefore, the results for frequency selective channels are not presented in this paper.

The cyclic prefix length in ePAM-DMT is limited by the total number of depths used. The maximum cyclic prefix length for ePAM-DMT, with a total number of depths D, can be given as:

$$N_{\mathrm{CP}}^{\mathrm{ePAM,max}} = \lfloor N/(2D-2) - 1 \rfloor. \tag{33}$$

This means that ePAM-DMT can be used for frequency selective channels only when the number of channel taps is less than $N_{\mathrm{CP}}^{\mathrm{ePAM,max}}$.

5.2. ASE-DMT with arbitrary constellation sizes

Arbitrary constellation sizes are proposed to close the remaining spectral efficiency gap between DCO-OFDM and ASE-DMT, when small number of depths is used for ASE-DMT. This would allow the spectral efficiency of ASE-DMT to be exactly similar to the spectral efficiency of DCO-OFDM with only few number of superimposed depths. Arbitrary constellation sizes offer a practical solution for ASE-DMT without any spectral efficiency loss. The computation complexity per bit associated with this approach is around 1.67 times higher than the computation complexity per bit of DCO-OFDM. Arbitrary constellation sizes would allow the non-squared constellation sizes of M-QAM DCO-OFDM to be achieved. For example, to achieve the spectral efficiency of 8-QAM DCO-OFDM, it would be possible to use 4-PAM at the first depth, 2-PAM at the second depth, and 4-PAM at the third depth of ASE-DMT. In order for the spectral efficiency of ASE-DMT to match the spectral efficiency of DCO-OFDM, the

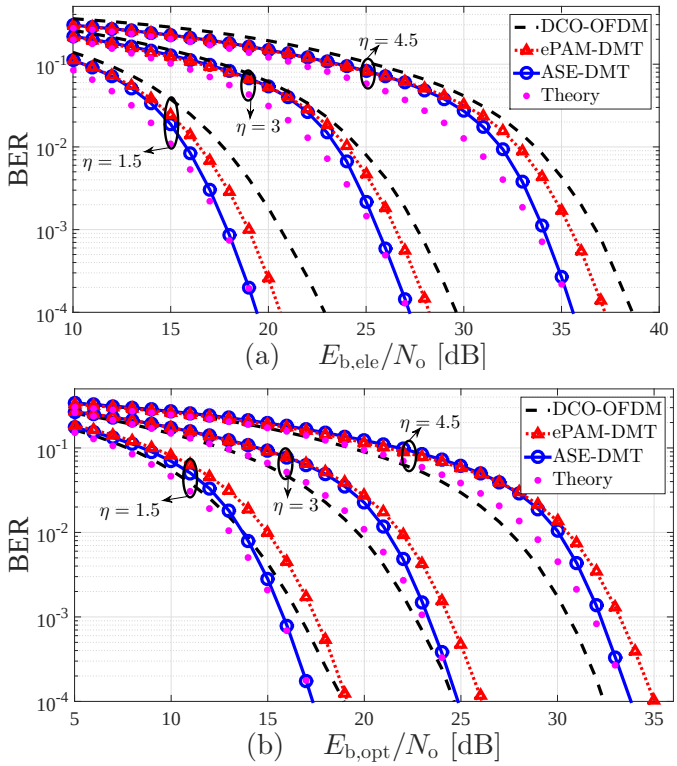

Fig. 8. The BER performance comparison of ASE-DMT, ePAM-DMT, and DCO-OFDM for different spectral efficiencies in an AWGN channel as a function of: (a) electrical SNR, and (b) optical SNR. The spectral effiency η is given in [bits/s/Hz]. The DC biasing levels for DCO-OFDM at $\eta = \{1.5, 3, 4.5\}$ are estimated through Monte Carlo simulations at respectively 7 dB, 9.5 dB, and 12 dB as described in (32).

combination of constellation sizes used should satisfy the following constraint:

$$\log_2(M_{\mathrm{DCO}}) = 2\sum_{d=1}^{D} \frac{\log_2(M_d)}{2^d}. \tag{34}$$

In addition, the power is allocated to each stream so that the average power of the modulation signal satisfies the following two constraints:

$$\begin{aligned} P_{\mathrm{Ele}}^{\mathrm{avg}}(D, \underline{\gamma}) &\leq P_{\mathrm{Ele}}^{\mathrm{avg}}(D, \mathbf{1}_{1\times D}), \\ P_{\mathrm{Opt}}^{\mathrm{avg}}(D, \underline{\gamma}) &\leq P_{\mathrm{Opt}}^{\mathrm{avg}}(D, \mathbf{1}_{1\times D}). \end{aligned} \tag{35}$$

The BER at each depth is weighted by the contribution of that depth to the overall spectral efficiency. The average BER performance can then be expressed as:

$$\mathrm{BER} \cong \sum_{d=1}^{D} \left(\frac{\mathrm{BER}_{(D,d,\underline{\gamma})}}{\alpha_\eta(D,d)} \right). \tag{36}$$

All possible combinations of constellation sizes at the different ASE-DMT depths with all possible power allocations are investigated for a maximum depth of $D = 3$, where spectral efficiency in the range from 1 to 5 bits/s/Hz is achieved. The optimal configurations were obtained

using Monte Carlo simulation comparisons of all the possible sets. The optimal configurations are presented in Table 3.

Since the performance of $\sqrt{M}$-PAM is equivalent to the performance of M-QAM, the resolution of the possible constellation sizes at each depth is limited. Fig. 8 presents the BER performance of ASE-DMT and DCO-OFDM as a function of electrical and optical SNR when arbitrary constellation sizes and scaling factors are used. The results are outlined in Table 3. In comparison to results outlined in Table 2, the approach of arbitrary constellation sizes reduces the electrical and energy gains of ASE-DMT. However, it increases the spectral efficiency of ASE-DMT at a reduced computation complexity. Therefore, a trade-off between the complexity and spectral and energy efficiencies for ASE-DMT is a function of the application required.

Table 3. The optimal combination of constellation sizes and scaling factors for ASE-DMT and the associated electrical and optical gains over DCO-OFDM at a BER of 10^{-4}, where M_d and γ_d denote the constellation size and the scaling factor for the modulation depth-d, respectively.

DCO-OFDM	η	ASE-DMT		Energy gains [dB]	
M_{DCO}-QAM	[b/s/Hz]	$\{M_1, M_2, ..., M_D\}$-PAM	γ [dB]	Ele.	Opt.
4-QAM	1	{2,2,4}-PAM	{1.9,2,-4.6}	0.6	-1
8-QAM	1.5	{4,2,4}-PAM	{-1.5,5.3,-1.2}	3.15	1.05
16-QAM	2	{4,8,4}-PAM	{2.4,-3.4,2.5}	2	0
32-QAM	2.5	{8,8,4}-PAM	{-0.9,-0.7,5.3}	3	0.75
64-QAM	3	{16,8,4}-PAM	{-2.7,3.2,9.4}	2.55	-0.25
128-QAM	3.5	{16,16,16}-PAM	{0,0,0}	3.28	0
256-QAM	4	{32,16,16}-PAM	{-2,3.6,3.7}	3.36	0
512-QAM	4.5	{32,32,64}-PAM	{1.5,1.7,-4}	3	-1.4
1024-QAM	5	{64,32,64}-PAM	{-1.3,4.3,-1.1}	4	-0.5

6. Conclusion

A novel energy efficient superposition modulation scheme for intensity modulation and direct detection (IM/DD) OWC is proposed. The scheme is based on selective frequency domain loading of M-PAM symbols, so that multiple streams can be superimposed and transmitted with no inter-stream-interference. The selective frequency domain loading of subcarriers allows low latency and simplified implementation of superposition modulation for PAM-DMT. The proposed scheme avoids the spectral and energy efficiency losses of ePAM-DMT.

The analytical bounds for BER performance are derived as a function of the electrical and optical SNR. The analytical bounds converge to match the Monte-Carlo simulations at high SNR values. The performance comparison shows the improvement of ASE-DMT over ePAM-DMT for the same spectral efficiency, and over DCO-OFDM at 87.5% of the spectral efficiency of DCO-OFDM for both electrical and optical SNR. A novel approach of arbitrary constellation sizes for ASE-DMT is proposed. This approach offers a simplified implementation of ASE-DMT with a reduced total number of depths. Future studies will include detailed comparisons with other superposition OFDM modulation schemes.

Acknowledgment

The authors acknowledge support by the UK Engineering and Physical Sciences Research Council (EPSRC) under Grants EP/K008757/1 and EP/M506515/1.